

HYBRID ACCRETION DISKS IN ACTIVE GALACTIC NUCLEI. I. STRUCTURE AND SPECTRA

AMRI WANDEL¹

The Hebrew University, Jerusalem; and Weizmann Institute of Science

AND

EDISON P. LIANG

Department of Space Physics and Astronomy, Rice University, Houston, TX 77251; and
Physics Department, Lawrence Livermore National Laboratory*Received 1989 November 13; accepted 1991 April 23*

ABSTRACT

We provide a unified treatment of the two distinct states of vertically thin AGN accretion disks: a cool ($T \sim 10^6$ K) optically thick solution, and a hot ($T_e \sim 10^9$ K, optically thin solution. We introduce a generalized formalism and a new radiative cooling equation valid in both regimes. We find a new luminosity limit $L < L_E$ at which the hot and cool α solutions merge into a single solution of intermediate optical depth. For the hot solutions we consider four cases: different ion and electron temperatures or ions and electrons in thermal equilibrium, with Comptonized bremsstrahlung or unsaturated Compton cooling. Analytic solutions for the disk structure are given, and output spectra are computed numerically. This is used to demonstrate the prospect of fitting AGN broad-band spectra, containing both the UV bump as well as hard X-ray and gamma-ray tail, using a single accretion disk model. Such models make definite predictions on the observed spectrum, such as the relation between the hard X-ray spectral index, the UV-to-X-ray luminosity ratio, and a ~ 1 MeV feature.

Subject headings: accretion — galaxies: nuclei

1. INTRODUCTION

In the study of vertically averaged thin accretion disks (hereafter TAD) models (e.g., Shakura and Sunyaev 1973; Novikov & Thorne 1974; Pringle & Rees 1972), it has been known that for most values of the accretion rate (or luminosity) and viscosity parameter, the steady state TAD structure equations admit two distinct solutions (e.g., Eardley et al. 1978). One corresponds to the standard optically thick, radiation pressure-dominated, low-temperature solution ($T \lesssim 10^5$ K for typical parameters; Shakura & Sunyaev 1973) commonly used to model the optical-UV emission of AGNs (Wandel & Petrosian 1988; Sun & Malkan 1986). The other one corresponds to the optically thin, gas pressure-dominated, high-temperature solution ($T > 10^9$ K; Eardley et al. 1978; Shapiro, Lightman, & Eardley 1976; Liang & Thompson 1979) commonly invoked to model the hard X-ray and gamma-ray emission of both AGNs and stellar mass black holes. Traditionally, the two solutions were obtained using two totally different formulations of the (vertical) energy transport equation, and the physical origin of the solution bifurcation is not transparent. For example, the radiative cooling equation for the optically thin case uses a mean temperature which is assumed to be identical to the effective radiation color temperature (cf. Shapiro et al. 1976), whereas the diffusion equation for the optically thick case uses an interior temperature which is distinct from the surface color temperature (cf. Shakura & Sunyaev 1973). There is no existing formula for a smooth transition from the optically thin to the optically thick case. In particular, without a formula applicable to all optical depths, we cannot address questions about the physical origin of the bifurcation, the possible existence or nonexistence of an

intermediate solution with moderate optical depth and the behavior of such a solution if it exists.

It is therefore highly desirable to have a unified treatment of the (vertical) radiation cooling equation referring to a single (electron) temperature which is valid for both the optically thick and thin cases. This will allow us a complete coverage of the parameter space to study the possible existence or non-existence of solutions with intermediate optical depths, and the transition from the optically thick to optically thin limits. Ultimately, it may also shed light on the time-dependent behavior and stability of the disk structure when the vertical optical depth is allowed to evolve in time.

In this paper we propose a well-behaved bridging formula for the vertical radiation cooling that is valid for all optical depths. Combining this equation with the rest of the TAD structure equations (see, e.g., Shakura & Sunyaev 1973; Liang & Thompson 1979), we derive the general solutions for the entire parameter space. We find that for most luminosity and viscosity values relevant to AGN disks, there is indeed a bifurcation of the solution into two and only two branches, one optically thin and hot, the other optically thick and cool. For the β -models in which the azimuthal stress is proportional only to gas pressure, we find no regime in which the two solutions merge into a single, intermediate optical depth solution. We also find that all hot optically thin β -model solutions are thermally unstable but secularly stable and all cool optically thick β -models are stable against both modes. However, the situation for the α -models in which the azimuthal stress is proportional to total (gas plus radiation) pressure, is more interesting and complicated. There are regimes of the parameter space in which there is zero, one or two solutions. Details of the α -models will be treated elsewhere. Here we only report some of the features of the bifurcated solutions in order to compare with the β -models. For the α -models, the hot optically thin branch is thermally unstable but secularly stable (e.g.,

¹ Postal address: Rakah Institute of Physics, The Hebrew University, Jerusalem, Israel.

Piran 1978; Liang & Thompson 1979), the radiation pressure-dominated cool branch is both thermally and secularly unstable (Shakura & Sunyaev 1976), and the gas pressure dominated-cool branch is stable against both modes.

The implication for AGNs, which exhibit both a strong UV bump and a hard X-ray and gamma-ray tail, is that the overall disk may be a hybrid one. One scenario would have the outer disk producing the optical-UV bump and the inner disk producing the hard X-ray-gamma-ray continuum. The relative strength of the two components would then be dictated by the radius separating the two solutions, in a manner similar to the scenario proposed by Thorne & Price (1975) for Cygnus X-1. Since the soft photons from the outer disk will impinge on the hot inner disk and regulate its temperature and optical depth, this luminosity ratio would also effect the X-ray-gamma-ray spectral index. Alternatively, the unstable cool disk may stabilize by pumping energy into a hot optically thin corona (Liang & Price 1977) and the coronal structure would again be governed by the optically thin solution. Such hybrid models would again predict a certain correlation between luminosity ratio and the X-ray-gamma-ray spectral index. Such predictions can be checked with future observations.

Section 2 gives an overview of the hybrid disk model. In § 3 we solve the unified disk equations in a generalized formalism, independent of the viscosity law, ion-electron coupling, or cooling mechanism. In § 4 we use this formalism to derive a new luminosity limit for α disks. Numerical solutions are discussed in § 5, and various limiting analytic solutions are listed in the Appendix. In § 6 we exhibit disk output spectra for the two branches of solutions. Sample spectra of hybrid models illustrating the relative strengths of the UV versus X-ray-gamma-ray continuum is presented in § 7. We summarize and review the stability analyses results in § 8. Section 9 is devoted to discussion and conclusions.

In our formulation of the equations and discussion of the solution properties for the optically thin case, we concentrate on models in which the radiation mechanism is dominated by Comptonization of self-emitted bremsstrahlung photons (cf. White & Lightman 1989) and derive explicit analytic solutions to the disk structure. Disk models with an external soft photon source, leading to unsaturated Comptonization, have been treated by previous authors (e.g., Shapiro et al. 1976; Liang & Thompson 1979) and are also summarized for comparison. We recognize that most observed AGN X-ray spectral indices (~ 0.5 - 2) are too soft to be compatible with Comptonized bremsstrahlung (index < 0). However, the study of such models is nonetheless relevant and useful because it provides a baseline reference point in which the soft photon source is known so that the solution is at least self-contained (i.e., the Kompaneets parameter γ is not an arbitrary free parameter). At the same time, its structure turns out to be not that different from the unsaturated Compton models.

We have restricted the energy coupling between electrons and ions in the hot optically thin solutions to classical Coulomb collisions (Spitzer 1962). But the behavior of the solutions if the electrons and ions are more tightly coupled (e.g., by collective plasma processes) is also investigated by varying the coupling constant as a fudge parameter (§ 4.3). We consider both α (stress = $\alpha \times$ the total pressure) and β (stress = $\beta \times$ gas pressure) models. Since the results are similar for the hot optically thin case, only the β -model solutions will be exhibited numerically and discussed in detail.

2. THE HYBRID DISK MODEL

The analyses in the following sections shows that the double-branched nature of the thin accretion disk model extends to almost all the relevant parameter space, as can be seen in the Σ - L/L_E (Eddington ratio vs. surface density) plane (Fig. 1). Given a cooling mechanism and the viscosity law, for every value of L/L_E (or equivalently, \dot{M}/\dot{M}_E), there are two and only two solutions: an optically thin (hot) solution, and an optically thick (cool) one. In principle, these two solutions can exist simultaneously, forming what we call a hybrid accretion disk.

The hybrid disk is very useful in modeling the continuum of quasars and active galaxies, as it can explain two different spectral regimes, the UV and hard X-rays, contrary to the simple accretion disk model, which can explain only the UV band in AGN. The reason for this difference is that the characteristic temperature of the thermal emission from a massive black hole disk (of the order of $10^8 M_\odot$) falls in the UV; hence the ordinary cool α disk cannot reach X-ray temperatures for AGN masses. In the hybrid model, on the other hand, a fraction of the UV photons from the cool disk are intercepted by the hot disk, and via inverse Compton scattering from the 2-100 keV power-law X-ray spectrum (Fig. 2). A further spectral component may emerge from those parts of the hot disk, which are shielded from the soft UV photons (see below). The quantitative details (e.g., the relative normalization of the UV and X-ray bands) depend on the geometry and must be determined numerically (§ 5).

We study three geometries for a hybrid accretion disk.

The stratified configuration (Fig. 3a).—The two solutions coexist at the same radii. A fraction of the accretion flow forms an optically thick, geometrically thin disk, while the rest of the material is in a hot, optically thin disk. Because the latter disk

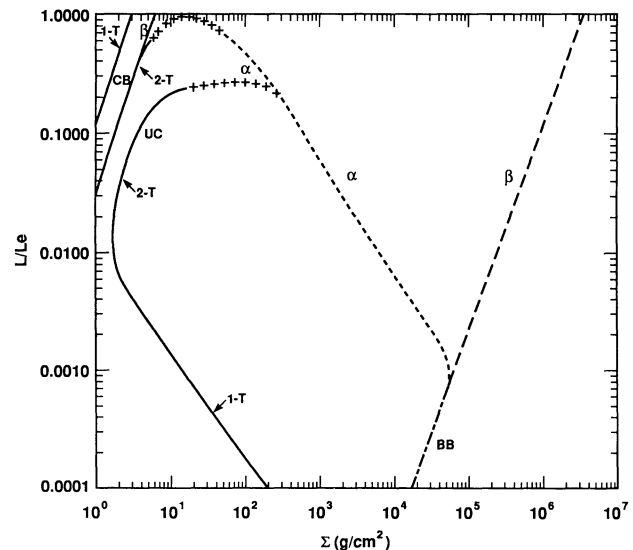


FIG. 1.—Behaviors of the different solution branches in the L - Σ plane at $r = 20$, $M_g = 1$, and $\alpha = 1$. CS denotes Comptonization of soft photons. CB denotes Comptonized bremsstrahlung (solid curves). Dotted curve is cool α solution and dashed curve is cool β solution. BB is the cool blackbody solution. Note that the α -solutions make a transition from positive to negative slope at $\Sigma \sim 10$ - 10^2 and $L/L_E \sim$ fraction (crossed sections are qualitative sketches only. Detailed behavior of this transition region will be reported in a separate paper [Liang & Wandel 1991]).

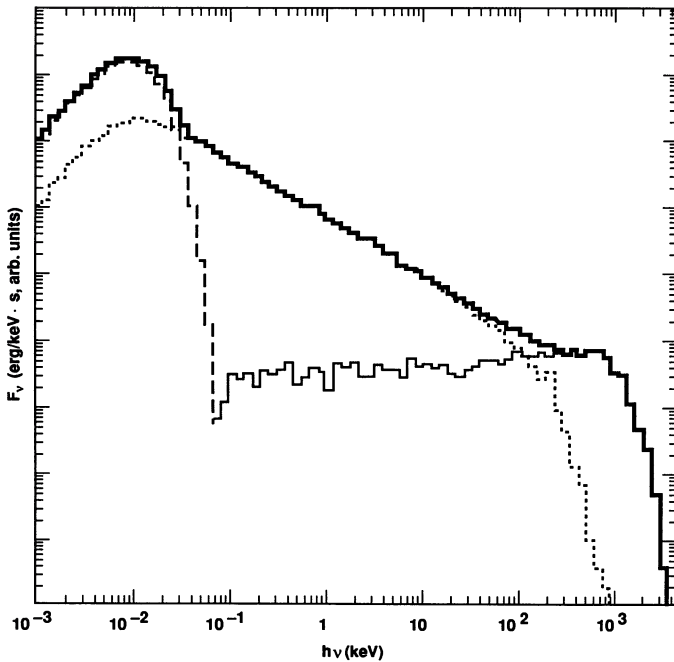
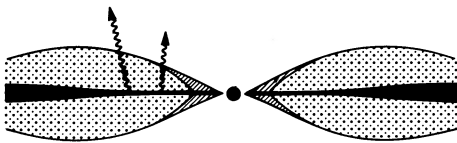


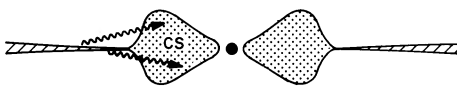
FIG. 2.—Output spectrum (heavy solid) of a $\beta = 1$, $L = L_E$ hybrid disk in which the cool disk occupies $r > 100$ (dashed), the Comptonized soft photon disk occupies $100 > r > 20$ (dotted), and the Comptonized bremsstrahlung disk occupies $r < 20$ (light solid). The luminosity ratio of the three components is approximately 1:3:3.

is much hotter, it has a larger scale height than the cool disk, extending as a corona above and below it, which may be referred to as the “sandwich geometry.” In this configuration, all the photons from the cool disk traverse the hot phase, and a fraction of them ($\sim \tau_{cs}$, if $\tau_{cs} < 1$) are Compton-scattered to form a power-law X-ray spectrum with a spectral index given by equation (27) below. This model has been suggested by

(a) “sandwich” geometry



(b) 2-zone radial geometry



(c) 3-zone radial geometry

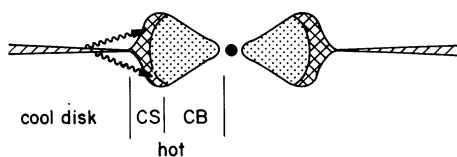


FIG. 3.—Hybrid accretion disk configurations

Wandel & Urry (1991) to fit simultaneously the UV and X-ray spectra of the BL Lac object PKS 2155-304.

The radial configuration (Fig. 3b).—The outer parts of the disk follow the optically thick solution, while the inner disk, which becomes radiation pressure-dominated and (for the α viscosity law) unstable, switches to the optically thin, hot solution, which is secularly stable. A fraction of the soft photons from the cool disk are intercepted by the hot inner disk and Comptonized to form an X-ray power-law spectrum. This kind of model was suggested by Shapiro, Lightman, & Eardley (1975, hereafter SLE) for Cyg X-1.

The three-zone radial configuration (Fig. 3c).—This is a variant of the radial configuration, which nevertheless produces a quite different spectrum in the 100 keV–1 MeV region. Although the hot disk is optically thin in the vertical direction, our numerical calculations show that often it is quite optically thick to electron scattering in the radial direction. The soft photons from the outer cool disk are therefore scattered by the outer parts of the hot disk, and the inner part of the hot disk is effectively shielded. Lacking the soft photons, this region will follow the Comptonized bremsstrahlung model derived below and will emit a flat spectrum with a knee at approximately 1 MeV (see Fig. 2), which may be observed in gamma rays.

3. UNIFIED ACCRETION-DISK ANALYSES

3.1. Disk Equations

The equations describing the accretion disk configuration have two solutions. One is the standard solution of a geometrically thin, optically thick disk (Shakura & Sunyaev 1973) with relatively low temperatures ($T \sim 10^6$ K). The other is a hot, two-temperature optically thin disk supported mainly by gas pressure of the ions, which reaches temperatures of $\sim 10^{11}$ K. In this case, Coulomb coupling often fails to equilibrate ion and electron temperatures, resulting in a lower electron temperature ($\sim 10^9$ K). The soft photon Compton hot accretion disk model was studied by SLE, but they assumed a fixed spectral index (Compton y -parameter ~ 1), while we leave it as a free parameter (η), which is then self consistently determined from the basic equations.

The physics describing thin accretion disks can be reduced to a system of five equations for five vertically averaged variables: density, scale height, energy flux, and ion and electron temperatures (ρ , h , F , T_i , T_e , respectively). These equations can be written in terms of the accretion parameters—the black hole mass M , the accretion rate \dot{M} , and the viscosity parameter α or β . The equations become simpler when the independent variable is chosen to be the Keplerian angular velocity (rather than the radius)

$$\omega = (GM/R^3)^{1/2} = 2.0 \times 10^{-3} M_8^{-1} r^{-3/2} \text{ s}^{-1}, \quad (1)$$

where $r = Rc^2/GM = R/1.5 \times 10^{13} M_8$ and $M_8 = M/10^8 M_\odot$, and \dot{M} is expressed in terms of the dimensionless luminosity:

$$L_* = \frac{\phi(r)L}{\epsilon L_E} = 0.4 \left(\frac{\dot{M}}{10^{26} \text{ g s}^{-1}} \right) M_8^{-1} \phi(r), \quad (2)$$

where ϵ is the efficiency ($= 0.057$ for an accretion disk around a Schwarzschild black hole), $L = \epsilon \dot{M} c^2$ is the total disk luminosity, and $L_E = 4\pi cGMm_p \sigma_T^{-1}$ is the Eddington luminosity. The function $\phi(r) = 1 - (r_0/r)^{1/2}$ is the correction at the inner edge, which is usually assumed at the marginally stable orbit around the black hole. $r_0 = 6$ for a Schwarzschild black hole

and $r_0 = 1.23$ for a maximally rotating Kerr black hole (e.g., Novikov & Thorne 1973).

The disk equations are given as follows.

3.1.1. Conservation of Energy

The rate of gravitational energy release by the accreted matter integrated over the vertical dimension

$$Q = \frac{3}{8\pi} \omega^2 \dot{M} \phi = 1.2 \times 10^{20} L_* M_8^{-1} r^{-3} \text{ ergs s}^{-1} \text{ cm}^{-2}. \quad (3)$$

At steady state this rate should be equal to F , the energy flux emitted from the disk surface per unit area, $Q = F$.

3.1.2. Hydrostatic Equilibrium

The pressure required to support the disk in the vertical direction is

$$P = \rho h^2 \omega^2. \quad (4)$$

The equation of state is

$$P = \rho k(T_i + T_e)/m_p + P_{\text{rad}}, \quad (5)$$

where T_i and T_e refer to ion and electron temperature, and P_{rad} is the radiation pressure. For radiative energy transport $P_{\text{rad}} = \tau_{\text{es}} F/c$, where $\tau_{\text{es}} = 0.4\rho h$ is the optical depth to electron scattering. In the case of thermodynamic equilibrium (when the effective optical depth, τ_* , is large) one can use the blackbody law, $P_{\text{rad}} = aT^4/3$, $\tau_* > 1$.

3.1.3. Viscous Stress

There are two common prescriptions for the viscosity: the standard α -disk, which assumes a viscous stress proportional to the total (gas plus radiation) pressure, and the “ β -disk” model, in which the viscosity is proportional to the gas pressure (Eardley & Lightman 1975). The latter case is relevant to the hot two-temperature model since, in most of the parameter space, the total pressure is dominated by gas pressure.

$$\dot{M}\omega\phi = 4\pi h\alpha P \quad \alpha \text{ disk}; \quad (6a)$$

$$\dot{M}\omega\phi = 4\pi h\beta P_{\text{gas}} \quad \beta \text{ disk}. \quad (6b)$$

3.1.4. Ion-Electron Thermal Coupling

At high temperatures, Coulomb coupling of ions and electrons may not be strong enough to achieve thermal equilibrium. In that case, their temperatures will differ, and flux is limited by the ion-electron coupling rate (Pringle, Rees, & Pacholczyk 1973; Guilbert & Stepney 1985)

$$F = \frac{3}{2} v_{ei} h \rho \frac{k}{m} (T_i - T_e)(1 + \Theta_e^{1/2}), \quad (7)$$

where $\Theta_e = kT_e/m_e c^2$ and

$$v_{ei} = 2.4 \times 10^{21} \ln \Lambda \rho T_e^{-3/2} = c_{ie} \rho T_e^{-3/2} \quad (8)$$

is the Coulomb coupling rate and the Coulomb logarithm $\ln \Lambda \sim 20$.

3.2. General Analytic Solution

We now derive a general analytic solution, by keeping the radiative transfer (eqs. [18a, b] below) and viscosity (eqs. [6a, b]) laws general as far in the derivation as possible. Equations (4) and (6a) give

$$4\pi\alpha\omega h^3 = \dot{M}\phi. \quad (9)$$

Equations (3), (6), and (7) give

$$\rho = \frac{\alpha\omega}{c_{ie}\Theta_*} T_e^{3/2}, \quad (10)$$

where $c_{ie} = 4.8 \times 10^{22}$ (in cgs units) and

$$\Theta_* = \frac{T_i - T_e}{T_i + T_e} (1 + \Theta_e^{1/2})(1 - P_*). \quad (11)$$

$P_* = P_{\text{rad}}/P$ is the radiation-to-total pressure ratio. For $T_e \ll T_i$ and $\Theta_e \lesssim 1$, Θ_* is of order unity if gas pressure dominates.

Equations (9) and (10) may be combined to derive an equation for h :

$$\frac{h}{R} = \left(\frac{c_{ie} \dot{M} \phi \Theta_*}{4\pi G M \alpha} \right)^{1/3} T_e^{-1/2} = 0.53 \alpha^{-2/3} L_*^{1/3} \Theta_*^{1/3} \Theta_e^{-1/2}. \quad (12)$$

Note that although we write the solution in terms of α , from equation (6) it is clear that the β solution can be easily obtained with α replaced by $\beta(1 - P_*)$.

Equations (9) and (10) can be substituted in the additional relation—the law of radiative transfer (e.g., eqs. [16] or [18a, b] below) to give a single equation for T_e . T_i is then found from equations (4), (5), and (9):

$$T_i + T_e = m k^{-1} \omega^2 h^2 (1 - P_*).$$

For $T_i \gg T_e$ this gives

$$\begin{aligned} \frac{kT_i}{m_i c^2} &= (1 - P_*) \left(\frac{h}{R} \right)^2 r^{-1} \\ &= 0.28 \alpha^{-4/3} L_*^{2/3} (1 - P_*) \Theta_*^{2/3} \Theta_e^{-1} r^{-1}. \end{aligned} \quad (13)$$

The left equation of the relation (13) demonstrates an important result: in a geometrically thin disk ($h \ll R$), T_i is guaranteed to be below the virial temperature, $kT_i < GMm_i/R = m_i c^2/r$.

Using equations (3) and (12) we can derive a general expression for the pressure ratio,

$$P_* = \frac{\tau_{\text{es}} F/c}{\omega^2 h^2 \rho} = 0.4 \frac{3\dot{M}\phi}{8\pi c h} = 47 \alpha^{2/3} L_*^{2/3} \Theta_*^{-1/3} \Theta_e^{1/3} \quad (14)$$

At low accretion rates or large radii, T_i approaches T_e and the two-temperature ($T_i > T_e$) solutions make a smooth transition to the one-temperature ($T_i = T_e$) solutions. In order to investigate this transition, it is useful to define the dimensionless ion-electron temperature difference, $\Delta_{ie} \equiv (T_i - T_e)/(T_i + T_e)$. Using equations (11)–(13), one can derive an equation for Δ_{ie} ,

$$\Delta_{ie} (1 - \Delta_{ie})^{3/2} = \left(\frac{2k}{m_i} \right)^{3/2} \left(\frac{4\pi\alpha^2}{c_{ie} \dot{M} \phi \omega} \right) \frac{(1 - P_*)^{-7/2}}{1 + \Theta_e^{1/2}} T_e^3. \quad (15)$$

Since these conditions usually also give relatively low electron temperatures, $1 + \Theta_e \approx 1$ and equation (15) may be solved for Δ_{ie} .

3.3. Radiative Transport and Cooling

Up to this point we did not specify the radiative transfer and cooling mechanism. In the optically thin limit, the equation of radiative transfer depends on the dominant cooling mechanism. We consider two cases: self-Comptonized thermal bremsstrahlung, and unsaturated Comptonization of external soft photons.

3.3.1. Self-Comptonized Thermal Bremsstrahlung

We assume the vertical energy transport is dominated by radiation. This implicitly assumes that energy transport by convection, magnetic, and acoustic waves, etc. is not important compared with radiative transport. This follows the traditional treatment in thin disks. In order to study the transition region between the optically thin and optically thick regimes and look for an eventual solution with an intermediate optical depth, we propose an interpolative formula which smoothly transits from the optically thick to the optically thin regime,

$$F = \frac{4}{3} \frac{AB(1 - e^{-\tau_*})}{[e^{-\tau_*} + (1 - e^{-\tau_*})A\tau_*]} \left(\frac{\tau_{\text{ff}}}{\tau_{\text{es}}} \right)^{1/2}, \quad (16)$$

where A is the Compton luminosity enhancement factor for bremsstrahlung defined below, $B = \sigma T_e^4$,

$$\tau_* = (\tau_{\text{ff}} \tau_{\text{es}})^{1/2} = 1.6 \times 10^{11} h \rho^{3/2} T_e^{-7/4} \quad (17)$$

is the effective optical depth, and τ_{ff} is the free-free Planck mean optical depth. This formula has three important properties:

1. It goes correctly to the diffusion limit $\tau_* \gg 1$

$$F = \frac{4}{3} \frac{B}{\tau_{\text{es}}}, \quad \tau_* \gg 1; \quad (18a)$$

2. It goes correctly to the optically thin limit when $\tau_* \ll 1$,

$$F = \frac{4}{3} B \tau_{\text{ff}} A = c_{\text{ff}} \rho^2 T_e^{1/2} h A, \quad (18b)$$

where $c_{\text{ff}} = 5.6 \times 10^{20} \text{ ergs s}^{-1} \text{ K}^{-1/2} \text{ g}^{-2} \text{ cm}^3$ is the bremsstrahlung emissivity coefficient;

3. F never exceeds the blackbody limit (eq. [18a]). It is seen that the transition from optical thinness to thickness is smooth, rapid, and insensitive to the exact value of τ_{es} or T_e .

In the optically thin case, the flux is given by the integrated free-free emission, enhanced by Compton scattering. The luminosity enhancement of radiation from thermal electrons Comptonizing their own bremsstrahlung is approximated by

$$A = \text{Max} \left[\frac{3}{4} \ln^2 \{ x_m [\ln(x_m^{-1})]^{1/2} \}, 1 \right]. \quad (19)$$

The frequency x_m is defined by

$$x_m = h\nu_m/kT = x_{\text{ff}} \text{Min} [1, (4kT\tau_{\text{es}}/m_e c^2)^{1/2}], \quad (20)$$

where

$$x_{\text{ff}} = 2.8 \times 10^{12} T_e^{-7/4} \rho h^{1/2} \quad (21)$$

(cf. Rybicki & Lightman 1979). While in the cool disk Comptonization is only marginally important (A is of order unity), it plays an important role in the hot disk. In most of the relevant parameter space, Comptonization is far from saturated, and we use a more accurate expression for A (Dermer, Liang, & Canfield 1991).

3.3.2. Comptonization of Soft Photons

In the presence of a copious soft photon source, cooling by Compton upscattering of the soft photons will dominate. Inverse Compton cooling is given by (Rybicki & Lightman 1979)

$$F_C = U_s c \text{Max} (1, \tau_{\text{es}}) y \text{ (ergs s}^{-1} \text{ cm}^{-2}\text{)}, \quad (22)$$

where

$$y = \tau_{\text{es}} (4\Theta_e + 16\Theta_e^2), \quad (23)$$

and U_s is the soft photon energy density. Equating the cooling to the energy flux from the disk we have $Q = \eta U_s c$, where η is the Compton enhancement factor. Assuming the cooling is dominated by inverse Compton we have

$$F = 4\eta^{-1} Q \tau_{\text{es}} \Theta_e (1 + 4\Theta_e). \quad (24)$$

When Comptonization is highly unsaturated, $\eta \approx e^y \approx 1 + y$. Note also that when $\Theta_e \sim 1$ the Fokker-Planck formalism we use becomes inaccurate, so we limit ourselves to $\Theta_e < 1$. Replacing equation (16) above by equation (24) the disk structure is solved analytically (cf. Shapiro et al. 1976; Liang & Thompson 1979). The analytic solution is given in the Appendix.

3.3.3. The Single-Temperature Disk

At low accretion rates (or large radii) the ion and electron temperatures of the 2-T hot solution become nearly equal (cf. Fig. 4). This is also the case if the thermal coupling between ions and electrons is much larger than Coulomb coupling (e.g. due to collective plasma processes; Begelman & Chiueh 1988). In this regime the correct solution can be obtained by setting $T_i = T_e = T$, ignoring equation (4) and solving equations (3)–(6) with equation (16) in the Comptonized bremsstrahlung case and with equation (24) in the Comptonized soft photon case. The solutions are given in the Appendix.

3.4. Solution of the Disk Equations

We have searched numerically for roots of the above equations and found that there are always two and only two roots for β disks (α -disk solutions are more complex; see next section). Despite the general form of equation (16), which in principle allows any arbitrary value of τ_* , one always finds one solution with $\tau_* \ll 1$ and the other $\tau_* \gg 1$. Hence in the following we will concentrate on the behavior of the solutions in the two limits.

Solving equations (3)–(8) and (16) for the optically thick limit reproduces the familiar thin disk solution (Shakura & Sunyaev 1973). For the optically thin limit, we are not aware of any full analytic solution of the Comptonized bremsstrahlung case.

Up to this point the solution is general, in the sense that we have not specified the cooling mechanism, or whether it is optically thin or thick. We now give the specific solution for the optically thin Comptonized bremsstrahlung cooling case (eq. [18b]). We will first assume the amplification factor A to be constant (this is justified because A is only slowly varying with the other variables, logarithmically). Combining equations (3), (9), (10), and (18b) gives an equation for T_e ,

$$T_e = \left(\frac{3}{2} c_{\text{ff}} A \right)^{-1/3} \left(\frac{\dot{M} \phi \omega}{4\pi \alpha^2} \right)^{2/9} (c_{\text{ie}} \Theta_*)^{5/9} \\ = (5.8 \times 10^{10} \text{ K}) \alpha^{-4/9} L_*^{2/9} A^{-1/3} \Theta_*^{5/9} r^{-1/3}. \quad (25)$$

Substituting in equations (10) and (12) gives

$$\rho = (5.8 \times 10^{-10} \text{ g cm}^{-3}) \alpha^{-4/9} L_*^{1/3} M_8^{-1} A^{-1/2} \Theta_*^{-1/6} r^{-2} \quad (26)$$

and

$$h = (2.6 \times 10^{12} \text{ cm}) \alpha^{-4/9} L_*^{2/9} M_8 A^{1/6} \Theta_*^{1/18} r^{7/6} \quad (27)$$

or, in terms of the radius, giving the opening angle of the disk,

$$h/R = 0.17 \alpha^{-4/9} L_*^{2/9} A^{1/6} \Theta_*^{1/18} r^{1/6}. \quad (28)$$

The Thompson depth is

$$\tau_{\text{es}} = 0.4 \left(\frac{\dot{M}\phi}{4\pi\alpha\omega} \right) h^{-2} = 600\alpha^{-1/9} L_*^{5/9} A^{-1/3} \Theta_*^{-1/9} r^{-5/6}. \quad (29)$$

Equation (13) gives the ion temperature (usually $T_i \gg T_e$)

$$T_i + T_e = (3.2 \times 10^{11} \text{K}) \alpha^{-8/9} L_*^{4/9} A^{1/3} \Theta_*^{1/9} r^{-2/3} (1 - P_*) \quad (30)$$

4. A LUMINOSITY LIMIT IN α -DISK MODELS

In the usual derivation of the α -disk analytic solution (e.g., Shakura & Sunyaev 1973), the equation of state is approximated by a single term (either gas or radiation pressure). The formalism developed above enables to keep both terms, which reveals an interesting property of the α -disk solutions.

The pressure-ratio term for the optically thin Comptonized bremsstrahlung case is

$$P_* = 143\alpha^{4/9} L_*^{7/9} A^{-1/6} \Theta_*^{-1/18} r^{-7/6} \text{ CB}. \quad (31)$$

In the Comptonized soft photon case equations (12) and (A3c) give

$$P_* = 12\eta^{1/4} \alpha^{7/12} L_*^{7/12} \Theta_*^{-1/6} r^{-7/8} \text{ CS}. \quad (32)$$

By substituting equation (11) into equation 31) or (32), we get an equation of the form

$$P_*(1 - P_*)^s = C(L/L_E)^a f(r), \quad (33)$$

where f , a , and b are defined so that $f(r) = \phi(r)^a r^{-b}$.

For β -models $s < 0$ [this is obtained by substituting in eqs. (31) and (32) $\alpha = \beta(1 - P_*)$], and equation (33) can be satisfied with $P_* \leq 1$ for any value of L/L_E . For α disks, however, the situation is different. There s is positive, and therefore the left-hand side of equation (33) has a maximum for $0 < P_* < 1$, and L/L_E is bounded. In other words, for large enough values of L/L_E , there is no solution satisfying $P_* < 1$. This introduces a new luminosity limit for hot α -disk models. In terms of equation (33), this limit may be written in the form

$$L/L_E < [C^{-1} P_*(1 - P_*)^s]^{1/a} \phi^{-1}(r) r^{b/a}, \quad (34)$$

where $0 < P_* < 1$ and s , a , b are positive. Evaluating equation (34) for the values of P_* and r that maximize the right-hand side, in both cases—CB and CS— $b/a = 3/2$, which for $\phi = 1 - (6/r)^{1/2}$ minimizes the function $\phi(r)r^{b/a}$ at $r = 32/3$. The maximum of the function $P_*(1 - P_*)^s$ occurs at $P_* = 1/(1 + s) = 0.80$ and 0.62 for the CB and CS cases, respectively. Equation (34) then readily gives the values of the maximal luminosity,

$$L_{\text{max}}/L_E = 0.18\alpha^{-7/18} A^{3/14} \text{ CB}, \quad (35a)$$

for models with bremsstrahlung, and

$$L_{\text{max}}/L_E = 0.80\alpha^{-1}\eta^{-3/7} \text{ CS} \quad (35b)$$

for soft photon Comptonization. In fact, when we solve the complete α -model equations with equation (16) instead of its optically thin limit, we find that the α -model bifurcates into the conventional $\tau_* \ll 1$ and $\tau_* \gg 1$ branches for $L \ll L_{\text{max}}$. As L increases, the two solutions approach each other and merge into a single, moderate τ_* solution at $L = L_{\text{max}}$, and there is no solution above L_{max} . This behavior is depicted in Figure 1, showing L/L_E versus surface density. Intuitively, the existence of this luminosity limit for α -models, which often could be sub-Eddington, is caused by the impossibility of the combined

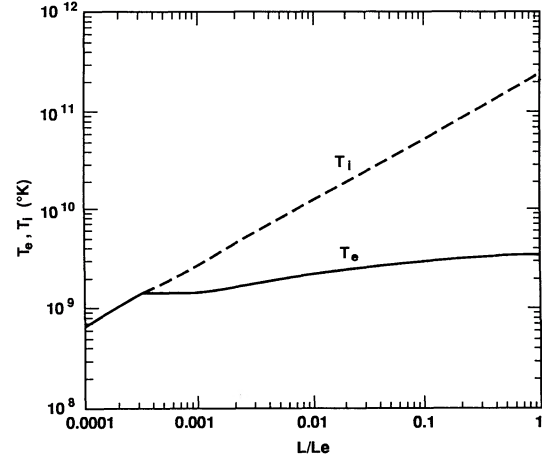


FIG. 4.—The ion (*dashed*) and electron (*solid*) temperature at $r = 20$ as a function of $L/L_E = \dot{M}/\dot{M}_{\text{crit}}$. In all figures we set $M_g = 1$ and $\alpha = 1$.

effect of radiation and gas pressure to satisfy hydrostatic equilibrium at high accretion rates. This failure usually occurs at such high column density and optical depth (Fig. 1) that the optically thin limit no longer applies. The correct behavior can only be studied using the full equation (16) valid for all optical depths. This new result is elaborated in a separate work (Liang & Wandel 1991).

5. NUMERICAL SOLUTIONS OF THE DISK STRUCTURE

5.1. Hot Disks

The structure of the Comptonized bremsstrahlung hot disk is calculated by solving numerically equations (3)–(8) and (16), with the Compton luminosity enhancement factor A taken from Dermer et al. (1991).

Figure 4 shows the variation of the ion (*solid*) and electron (*dashed*) temperatures with L/L_E at a fixed radius, while Fig. 5 shows the temperature profiles for $L/L_E = 1, 0.1$, and 0.01 . Note that the electron temperature is $2\text{--}3 \times 10^9$ K, almost independent of L_* and of radius, while T_i decreases with radius and with Eddington ratio. For a large enough radius, and for a low enough accretion rate, T_i decreases enough to become equal to T_e . From Figure 7 we see that this happens at $r = 40$ for $0.01L_E$ and at $r = 200$ for $0.1L_E$.

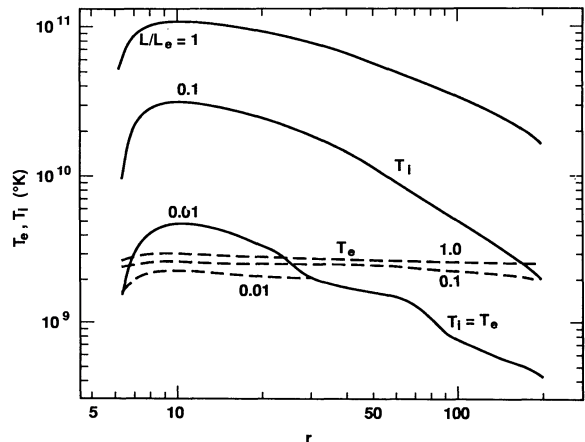


FIG. 5.—The ion (*solid*) and electron (*dashed*) temperature profiles for the hot Comptonized bremsstrahlung two-temperature disk, $M_g = 1$ and $\alpha = 1$.

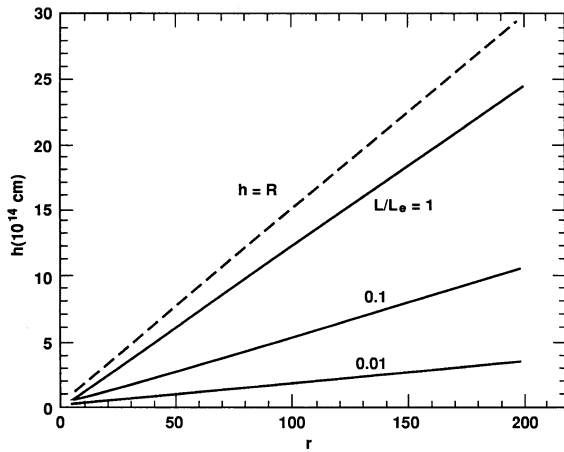


FIG. 6.—The scale height of the hot disk vs. radius for $L/L_E = 1, 0.1,$ and 0.01 . The dashed line marks a configuration with a 45° opening angle ($h = R$).

The scale height versus the radius is shown in Figure 6. The thin disk assumes the disk is geometrically thin, but we see that for luminosities close to the Eddington luminosity, $h \sim R$, as can be seen from Figure 6 and from equation (28). For $L = L_E$, the disk has an opening angle of $\sim 40^\circ$.

The hot disk model is marginally optically thick to electron scattering, as can be seen from Figure 7. This results from the fact that these disks have a much lower surface density than their cold counterparts. The relative surface density of the hot and cold solutions can also be seen in the Σ versus L/L_E plane (Fig. 1).

Figure 8 shows the variation of the Compton enhancement factor with radius for several values of L/L_E . As expected, it is not very sensitive to the parameters— $A \sim 300$ for $L = L_E$ and decreases approximately as $(L/L_E)^{1/2}$. The rapid decrease near $r = 100$ for $L = 0.01L_E$ is caused by the fall in T_e when it becomes equal to the ion temperature.

The hot disk solutions are mostly dominated by gas pressure throughout. Because of this reason, the α disks do not differ much from the β ones, since $P \sim P_{\text{gas}}$. Figure 9 shows the

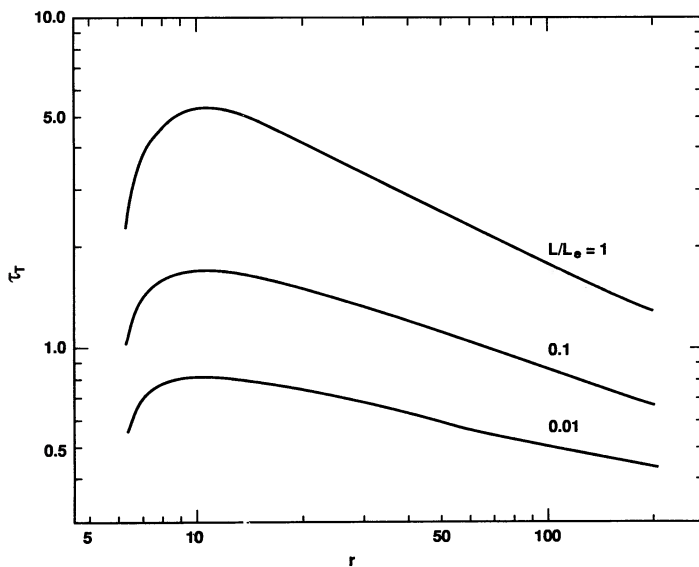


FIG. 7.—The Thomson scattering optical depth of the hot disk vs. radius for $L/L_E = 1, 0.1$ and 0.01 .

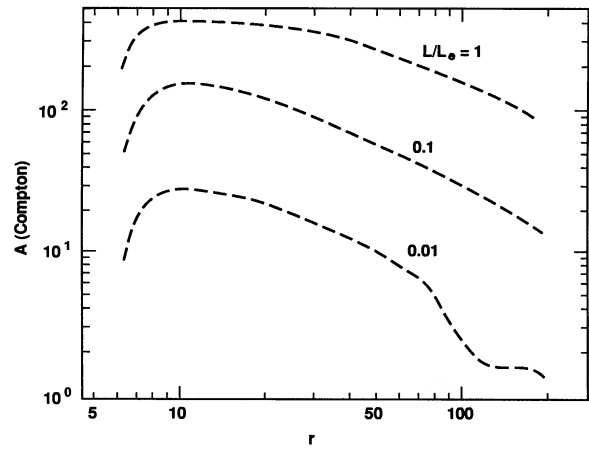


FIG. 8.—The Compton amplification factor of bremsstrahlung as a function of radius for hot accretion disk with various L/L_E .

dependence of the gas-to-radiation pressure ratio for β disks with $L/L_E = 1, 0.1,$ and 0.01 . An exception occurs for near-Eddington disks at small radii, where $P_{\text{rad}} > P_{\text{gas}}$. In that regime the α solution differs significantly from the β one, as discussed in § 2.3.

The Comptonized bremsstrahlung hot solution has also been treated by Kusonose & Takahara (1989) and White & Lightman (1989) who include also the effects of electron-positron pairs. However, they did not give the explicit functional dependence and analytic solutions which we provide in the Appendix, nor do they discuss the spectrum.

5.2. Cool Disks

For comparison we have also reproduced the cool disk solutions. In this case we concentrate on the inner, radiation pressure-dominated regime, since that is where the maximal temperature is reached, and, for reasonable parameters, also where the bulk of UV and eventually soft X-ray photons are emitted. We use the α and β solutions for the disk structure in the optically thick regime, while the surface temperature (which in the optically thin case is also the disk temperature) is calculated by a recursive solution of the energy equation,

$$F(R) = \pi \int I_\nu(T, \rho, \tau) d\nu, \quad (36)$$

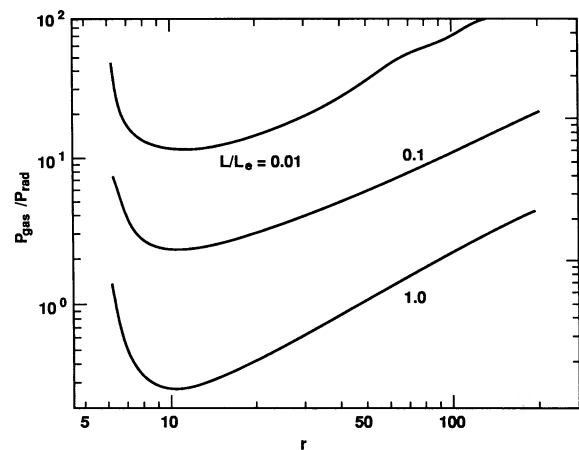


FIG. 9.—The gas-to-radiation pressure ratio vs. radius for $L/L_E = 1, 0.1,$ and 0.01 hot disks.

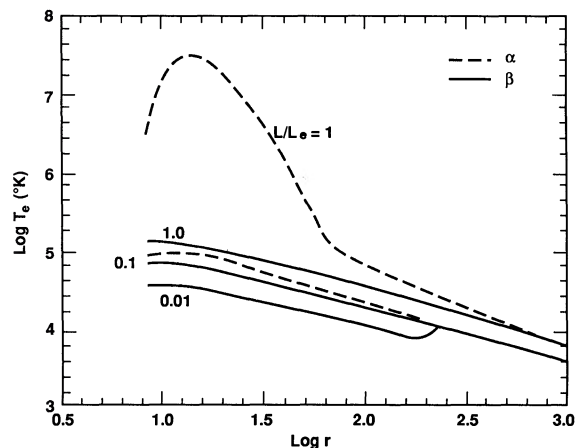


FIG. 10.—The temperature profiles for cool α (dashed) and β (solid) disks

using an interpolative formula for the spectrum (Wandel & Petrosian 1988), which goes to the modified blackbody spectrum for a high effective optical depth, and to the Comptonized bremsstrahlung form for a low optical depth.

Figure 10 shows the temperature profiles for the α (dashed curve) and β (solid curve) cold disks for $L/L_E = 1, 0.1$, and 0.01 . The steep increase in the temperature of the α model with $L = L_E$ is due to the inner part becoming optically thin; hence the energy is radiated via Comptonized bremsstrahlung, which is much less efficient than a modified blackbody spectrum. The transition to the optically thin regime can be seen in Figure 11, which shows the dependence of the effective optical depth on radius. As we have discussed above, the hot and cool α solution join into a single solution of intermediate τ_* (cf. Fig. 1).

5.3. Dependence on the Ion-Electron Coupling

We have assumed Coulomb coupling in the hot solution. If the ion and electron temperatures differ greatly, plasma effects are likely to cause increased coupling (e.g., Begelman & Chiueh 1988). We attempt to investigate this effect by increasing the

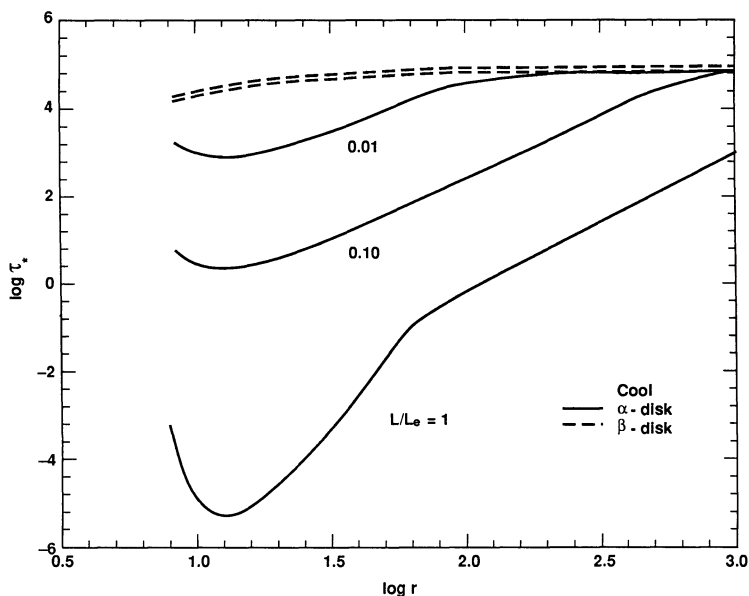


FIG. 11.—The effective optical depth for cool α (solid) and β (dashed) disks

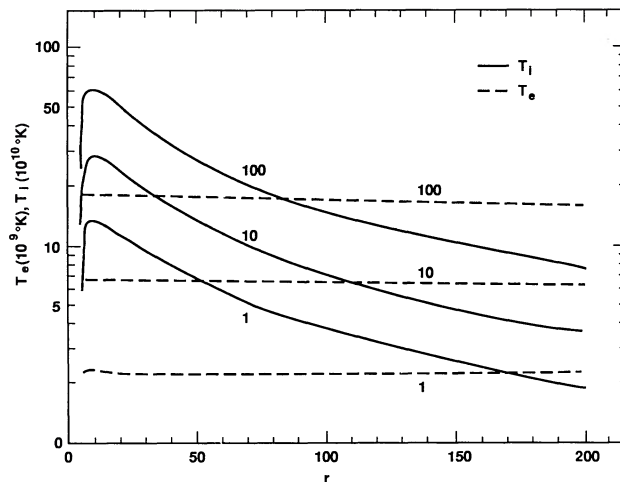


FIG. 12.—Ion and electron temperature profile for 1, 10, and 100 times Coulomb coupling for the hot Comptonized bremsstrahlung disk.

coupling constant c_{ie} . From equation (25) we see that T_e increases with the coupling constant as $c_{ie}^{5/9}$. However, from equations (12), (13) it follows that also the ion temperature increases with the coupling constant as $c_{ie}^{2/3}$, that is by nearly the same amount. This result can also be seen from Figure 12, which shows the ion and electron temperatures for hot bremsstrahlung disks with 1, 10, and 100 times the Coulomb coupling. This counterintuitive effect is a result of the disk equations and is understood by noting that the coupling rate ν_{ie} is actually very weakly dependent on c_{ie} . In reality, the ion temperature cannot increase beyond the virial temperature. When the ion-electron coupling is increased, the ion and electron temperatures approach the single-temperature (1-T) hot solution. A more rigorous treatment of modified ion-electron coupling in 2-T hot accretion disks is given in Wandel & Litwin (1991).

5.4. Pair Processes

So far we have neglected effects of electron-positron pairs. A priori it is not clear this is justified, as electron temperature does approach the electron rest mass. These effects were taken into account in detail by White & Lightman (1989; see also Kusonose & Takahara 1989), who find two solution branches: one with low pair density ($z \equiv n_+/n_p \ll 1$) and one with high-pair density $z \gtrsim 1$. Clearly in the low-pair density branch, our results remain valid to the order of $O(z)$. We cannot say much on the high-pair density branch, unless pairs are included in the disk equations as given in White & Lightman. However, in that case, the complexity of the expressions for the pair interactions prevent explicit analytic solutions.

Pair processes could affect the overall structure of the hot solution, and we should ask if they modify the luminosity limit presented in § 4. In particular, for the Comptonized hot bremsstrahlung hot solution, White & Lightman (1989) found that pair balance imposes a more stringent luminosity limit than L_{\max} given in equation (35a). However, their models assume gas pressure domination and a thin disk approximation, which may not be totally consistent. Liang (1991), on the other hand, assuming a pair cloud with quasi-spherical geometry and including both gas and radiation pressure, finds a luminosity limit similar to that of equation (35). It is safe to say that while the quantitative impact of pair effects remains unsettled, the qualitative result of the existence of L_{\max} at the

gas radiation pressure transition seems insensitive to the inclusion of pairs. For the soft photon Comptonization case, White & Lightman (1989) found no major pair effects, nor a luminosity limit due to pairs, so the luminosity limit due to gas radiation pressure transition is expected to remain roughly the same.

6. MODEL OUTPUT SPECTRA

In this section we contrast the properties of the cool, optically thick solutions and the hot, optically thin solutions for the same parameter space by showing their respective output spectra. These are obtained by computing the local spectrum for each radius r and then integrating over the relevant radii. The cool, optically thick disk spectra have been previously discussed in Wandel & Petrosian (1988) and are reproduced here for comparison. For the hot optically thin case, we show sample spectra of both the Comptonized bremsstrahlung solutions discussed in § 5 as well as the unsaturated Compton solutions first discussed by Shapiro et al. (1976) in the context of Cyg X-1 and generalized by Liang & Thompson (1979, reproduced here in the Appendix). As we have discussed in the Introduction, the hot Comptonized bremsstrahlung spectra are generally too hard to fit the AGN spectra observed so far (Rothschild et al. 1983). They are included here for completeness. The unsaturated Compton spectra depend on the amount of copious soft photons supplied internally or externally and their power law slope is a free parameter. In the next section we will try to combine the cool, optically thick solution and the hot, unsaturated Compton solution into a single-disk model and see if the combined spectra of the hybrid model can be consistent with both the observed UV and X-ray–gamma-ray spectral data of AGNs. Throughout these two sections for the general solution we will limit ourselves to β -models only since the cool α disk is unstable and there is a regime where there is no solution at all (cf. § 3.3). All of the hot disk model spectra were generated with the LLNL relativistic Monte Carlo radiation code (Canfield et al. 1988). Figure 13 illustrates the typical spectra of the cool, optically thick solutions for the case $\beta = 1$ and three sample values of L_* . They all have a modified blackbody shape (broadened by the radial distribution, of course) and peak in the UV (10^{15} – 10^{16} Hz). In contrast, Figure

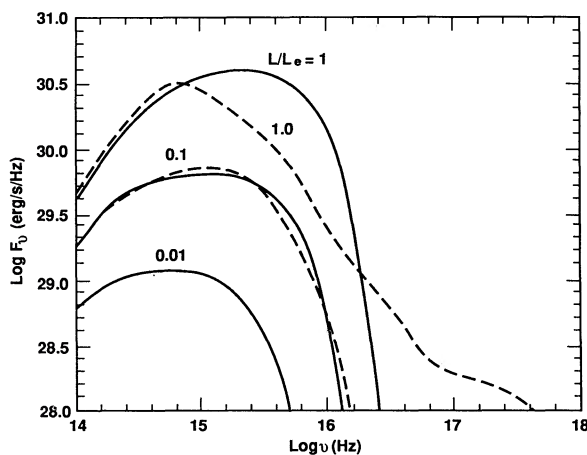


FIG. 13.—Spectra of cool α (dashed) and β (solid) disks for $L/L_E = 1, 0.1,$ and 0.01 . For $L < 0.1L_E$ the α and β spectra converge to the multiblackbody disk spectrum.

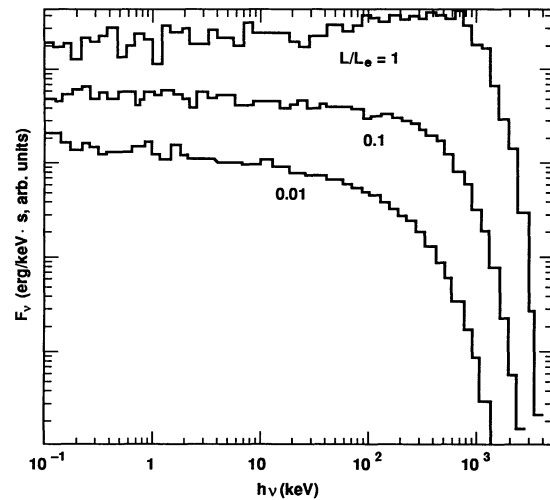


FIG. 14.—Spectra of Comptonized bremsstrahlung disk for $L/L_E = 1, 0.1,$ and 0.01 hot disks. The spectra are calculated by the relativistic Monte Carlo method with $M_g = 1$ and $\alpha = 1$.

14 shows typical spectra of the hot, optically thin, Comptonized bremsstrahlung solutions for the same parameters. We see that for low L_* the spectra are flat in the X-rays and cut off exponentially at a few hundred keV. But for the $L_* = 1$ case the spectrum develops a conspicuous Wien hump at soft gamma-ray energies due to the high Thomson depth (cf. Fig. 7). Of course, when the temperature and Thomson depth are as high as in this case, pair production should start to become important and the requirement of pair balance (e.g., Svenson 1984) would lower the effective temperature or Thomson depth. But the lowering of the Wien lump is compensated by the contribution of the broadened pair annihilation feature so the true spectral shape including pair contributions is in fact very similar to that given here, as found by Liang & Dermer (1988; also Zdziarski 1984) for the Cygnus X-1 case (Ling et al. 1987). The detailed discussion of pair-dominated disks is beyond the scope of this paper (see, e.g., White & Lightman 1989; Kusunose & Takahara 1989). Even though the temperature, density, and Thomson depth profiles of the unsaturated Compton disk models differ only mildly from those of the Comptonized bremsstrahlung solutions (cf. Appendix), the output spectra of such disks are totally different, because in this case the spectral shape becomes completely regulated by the amount of soft photons injected into the Comptonizing region, and the contribution of the bremsstrahlung photons is negligible. Figure 15 gives some sample unsaturated Compton output spectra for a variety of disk model parameters, ranging from very low Compton enhancement factor η (cf. Dermer et al. 1991) to Compton enhancement factors of several hundred. Note that the spectra are typically power laws in the X-rays with an exponential cutoff at a few hundred keV. The power-law indices ($I_\nu \propto \nu^{-n}$) are related to the Thomson depth and electron temperature through the well-known formula (Pozdnyakov, Sobol, & Sunyaev 1976).

$$n = \left(\frac{9}{4} + 4y^{-1} \right)^{1/2} - \frac{3}{2} \quad y = \frac{4kT_e}{m_e c^2} \frac{12(\tau_{es} + 2/3)^2}{\pi^2}. \quad (37)$$

They lie in the range ≈ 0.3 – 2 for current model parameters. All the model spectra discussed so far are for a single-solution branch covering the entire range of radius. In the next section, we will consider spectra of hybrid solutions in an attempt to

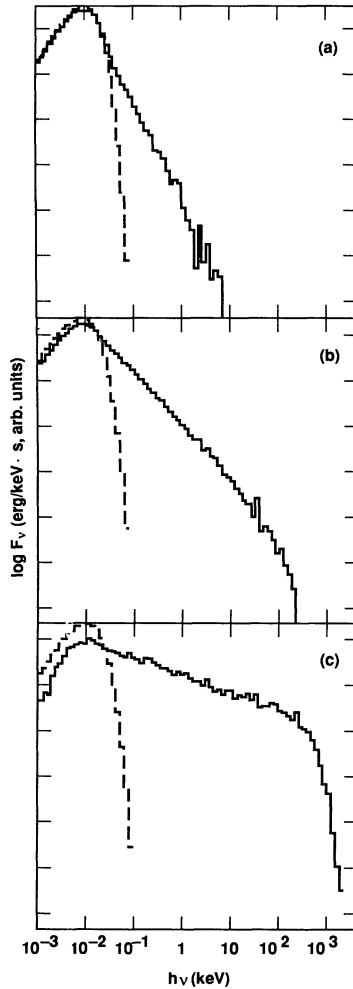


FIG. 15.—Comptonized soft photon disk spectra for (a) $\tau_{es} = 0.1$, $T_e = 8 \times 10^8$ K, $h = 1.15$; (b) $\tau_{es} = 0.6$, $T_e = 5 \times 10^8$ K, $h = 3.5$; and (c) $\tau_{es} = 1$, $T_e = 3 \times 10^9$ K, $h = 340$. Dashed curve shows injected soft photon spectrum. In the context of the stratified disk-corona model, dashed spectrum represents output of cold disk, and solid curve, the total disk-corona output.

model simultaneously the UV bump and the X-ray–gamma-ray continuum.

7. SPECTRA OF HYBRID MODELS

Since most of the observed AGN spectra exhibit both a UV bump and a power-law X-ray–gamma-ray continuum, it is tempting to try to associate the two spectral components with the two-solution branches. There are two natural, naive ways to construct such hybrid models that we will consider here. One approach is to associate the hot optically thin solution to the inner region of the disk and the cool optically thick solution to an outer region of the disk, similar to the concept of Thorne & Price (1975) or Shapiro et al. (1976) for Cyg X-1. In this case both the amount of external soft photons impinging on the hot inner disk and the ratio of UV to X-ray–gamma-ray luminosities are determined by the separation radius of the two regions. The other approach is to assume that both solutions coexist at all radii, with the hot optically thin solution forming a hot corona engulfing the cool optically thick disk (e.g., Liang & Price 1977; Liang & Thompson 1979). In this case, all of the soft photons from the cool disk must pass through the

hot Comptonizing region. Hence both the ratio of the UV to X-ray–gamma-ray luminosities and the X-ray–gamma-ray spectral index are determined by the Compton enhancement factor η , or effectively, the relative amounts of energy generated in the cool disk versus the hot corona. While both models predict a hardening of the X-ray–gamma-ray spectrum as the ratio of UV to X-ray–gamma-ray luminosity goes down, each case predicts a different quantitative relation between the two observables. Future observations should be able to test this. Here we will only discuss the basic theoretical results and show some sample spectra but leave the detailed comparison with observational data to future papers. Figure 16 illustrates the combined spectral output of a radially segregated $L_* = 1$, $\beta = 1$ solution where the cool outer disk and hot inner disk are separated at $r = 24$, corresponding to equal luminosities for both components. We use the unsaturated Compton disk model to estimate the opening angle of the hot disk as seen by the cold outer disk and estimate by hand the fraction of cool blackbody photons impinging onto the inner disk at each radius. The output of the inner disk is then computed as the reflection spectrum of a scattering medium of the appropriate Thomson depth. The fraction of UV cool disk photons impinging onto the hot inner disk is roughly 10%, and these far exceed the self-emitted hot bremsstrahlung photons by $\sim 10^4$. Hence, the hot inner disk is an unsaturated Compton solution (cf. Appendix). The resultant X-ray–gamma-ray spectrum has an index of ~ 1 and a Compton enhancement factor of ~ 10 . This represents the midrange of the AGN spectral distributions. The unsaturated Compton spectra of Figure 16 also represent the output of stratified hybrids model with a hot corona sandwiching the cool disk. Note that in this case in order for the UV and X-ray–gamma-ray components to have similar luminosities, the X-ray spectral index has to be much softer (~ 1.5 – 2), close to the soft end of AGN spectral distributions. This is because all soft photons pass through the corona, and the spectral index is simply related to the Compton enhancement factor (Pozdnyaykov et al. 1976). Future coordinated multiwavelength observations of AGNs should be able to distinguish between the two types of hybrid configurations. While the hot Comptonized bremsstrahlung model has an X-ray spectrum too hard to agree with most observed AGN data, we should not dismiss them as being never relevant to useful hybrid configurations. If the radial separation radius of the hot and cold regions goes out to sufficiently large values, say $r > 100$ (so that the UV component is weak), then since the soft photons can only penetrate a few Thomson depths radially, there may remain a substantial inner disk not dominated by external soft photons. In this case we will have a hybrid model of three regions: a hot Comptonized bremsstrahlung inner disk with few additional soft photons, a middle hot unsaturated Compton disk dominated by external soft photons from the outer disk, and a cool outer disk. Figure 2 illustrates the combined output of such a hybrid model. Here the spectral output of the two outer regions are computed as in Figure 16, but the ultrahot Comptonized bremsstrahlung central region is approximated as a sphere since its scale height is comparable to r . Note that while the X-rays are primarily emitted by the unsaturated Compton region, giving a power law-spectrum, the gamma rays are dominated by the Comptonized bremsstrahlung emission. Such spectrum may correspond to the gamma-ray state of some AGNs (e.g., NGC 4151 and 3C 273) as well as Galactic black hole candidates (Cyg X-1 and Galactic center). As we have discussed previously, the

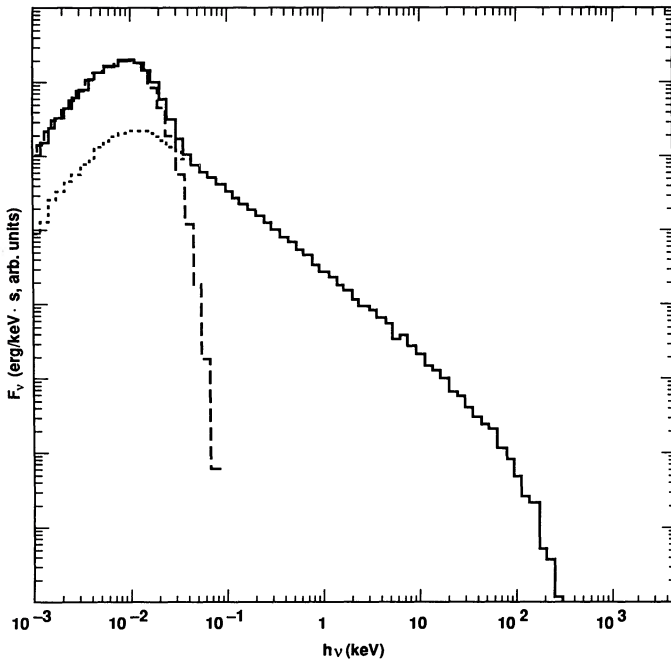


FIG. 16.—Output spectrum (solid curve) of a $\beta = 1$, $L = L_g$ hybrid disk in which the cool disk occupies $r \geq 24$ (dashed) so that the two components have equal luminosities.

actual origin of the gamma continuum must involve pair processes which we have neglected here (Liang & Dermer 1988). But the net spectral output of the resultant pair-balanced solutions turns out to be not that different from the sample spectra shown here since the lower Thomson depth required by pair balance (e.g., Svensson 1984; Zdziarski 1984) compensates the additional contribution from pair annihilation (Liang & Dermer 1988) for most of the parameters relevant to the current models.

8. STABILITY ANALYSES

One of the simplest, conventional ways to look at local secular instability of thin accretion disks is to plot the accretion rate versus the vertical column density Σ (or equivalently, Thomson depth). Then the disk is said to be secularly stable (or unstable) if the slope is positive (or negative; see, e.g., Clarke 1988). In Figure 1 we plot the L_* (which is proportional to \dot{M}/M) versus Σ for the different solution branches discussed in § 3 for both α and β models. It is clear that all β models are secularly stable according to this limited definition, whereas the α models have a very interesting behavior which is being reported in a separate paper (Liang & Wandel 1991). At least for some values of α and r , above a certain critical L_* , there is no solution at all. There is a single solution with $\partial L/\partial \Sigma = 0$ at the critical L_* and below the critical L_* there are the two well-known solutions: the cool optically thick radiation pressure-dominated solution which is secularly unstable (Lightman & Eardley 1974) and the hot optically thin gas pressure dominated-solution which is secularly stable. At very low L_* the cool α solution becomes gas pressure-dominated again and is stable, merging with the β solution into the blackbody disk. Even when the disk is locally secularly stable it may still be thermally unstable (Pringle 1976; Shakura & Sunyaev 1976) or unstable to global modes (Papaloizou & Pringle 1984). The investigation of global instability for the different

solutions is beyond the scope of this paper. Here we concentrate on the local instabilities. As pointed out by Shakura & Sunyaev (1976) both the thermal and secular instabilities can be studied within a single framework by comparing the partial derivatives of the heating and cooling energy flux with respect to scale height h and column density Σ . Here we repeat that analyses for the current solutions using the formalism of Piran (1978), Sakimoto & Coroniti (1981), and Liang & Thompson (1979).

Define $j = \partial \ln Q_- / \partial \ln h$ and $l = \partial \ln Q_- / \partial \ln \Sigma$ where Q_- is the vertical cooling energy flux. For all α -models and also β -models dominated by gas pressure, if $2l - j > 0$ then there is one stable (secular) mode and one unstable (thermal) mode; if $2l - j < 0$ then both modes are stable if $j > 2$ and both unstable if $j < 2$ (for the origin of these criteria see Piran 1978 or Liang & Thompson 1979). However, for β -models dominated by radiation pressure, then the secular mode is stable and thermal mode is unstable if $l - 5j > 0$. If $l - 5j < 0$ then both modes are stable if $j > \frac{1}{4}$ and both are unstable if $j < \frac{1}{4}$. We now compute j and l for the different solutions.

1. Two-temperature Comptonized bremsstrahlung.

$$Q_- \propto Ah\rho^2 T_e^{1/2} \propto T_i \rho^2 h T_e^{-3/2} (1 + \Theta_e^{1/2}) \quad (38)$$

where

$$T_i \propto h^2 (1 - Ch^{-1}) \quad C = \text{const} \leq h.$$

From this we find $\partial \ln T_e$ in terms of $\partial \ln h$ and $\partial \ln \Sigma$. After some algebra we obtain:

$$j = 1 - \frac{3}{2} \left[1 + L + \frac{1}{2} \frac{C}{(h - C)} \right] \cdot \left[\frac{1 + T_*^{1/2}}{1 + 3T_*^{1/2}/4} \right], \quad (39)$$

$$l = 2 - \frac{3}{2} K \left[\frac{1 + T_*^{1/2}}{1 + 3T_*^{1/2}/4} \right], \quad L, K \sim \frac{1}{A^{1/2}} \ll 1.$$

Hence $2l - j > 0$ for all T_* and h .

2. $T_i = T_e$ Comptonized bremsstrahlung hot solution.

$$Q_- \propto Ah\rho^2 T_e^{1/2}; \quad T_e \propto h^2. \quad (40)$$

We obtain

$$j = L \quad \text{and} \quad l = 1 + K. \quad (41)$$

Since

$$L, K \sim \frac{1}{A^{1/2}} \ll 1,$$

again we have $2l - j > 0$.

3. Unsaturated Compton with fixed soft photon source (cf. Liang & Thompson 1979).

Define $k = \partial \ln \eta / \partial \ln y$ so that $k = y$ in the limit $\eta \cong e^y$ at low y .

In the $\tau_{es} < 1$, $T_i \gg T_e$ regime,

$$j = k_0 / (\frac{3}{2} + k_0); \quad l = 7k_0 / 2(\frac{3}{2} + k_0). \quad (42)$$

In the $\tau_{es} > 1$, $T_i \cong T_e$ regime,

$$j \cong 2k_0 \cong l \quad (43)$$

where k_0 is unperturbed value of k . Hence we have $2l - j > 0$ for both regimes.

4. Cool gas pressure-dominated solutions (α or β model; Piran 1978)

$Q_- \propto T^4 \Sigma^{-1} \cdot T \propto h^2$ (hydrostatic balance). Hence $j = 8$,

$l = -1$. We obtain $2l - j < 0$ and $j > 2$. Hence both modes are stable.

5. Cool alpha radiation-pressure-dominated solutions (cf. Pringle 1976; Shakura & Sunyaev 1976).

$Q_- \propto T^4 \Sigma^{-1}$, $T^4 \propto \Sigma h$. We obtain $j = 1$, $l = 0$. Hence $j < 2$ and $2l - j < 0$. Both modes are unstable.

6. Cool beta radiation-pressure-dominated solutions: $Q_- \propto T^4 \Sigma^{-1}$, $T^4 \propto (\Sigma h)^{1/4}$.

We obtain $j = 1$, $l = 0$. Hence $l - 5j < 0$ and $j > \frac{1}{4}$. Both modes are stable.

Hence for all optically thin hot solutions we find that the solution is secularly stable but thermally unstable. All cool optically thick gas pressure-dominated solutions are secularly and thermally stable. But the cool radiation dominated α -models are thermally and secularly unstable. The severity of thermal instability and the level at which they will saturate is a subject of debate. We do not believe that such issues can be settled within the context of thin vertically averaged disk models.

9. DISCUSSION AND SUMMARY

In this paper we have provided a unified treatment of both the cool optically thick and hot optically thin solutions of AGN accretion disk models. Since each solution branch is relevant to a different component of the observed spectra (UV versus X-rays-gamma-rays), we attempt to address the issue of explaining both spectral components within a single disk framework using hybrid models. Synthesizing composite spectra for such models, we find that different configuration (radially segregated vs. vertically stratified) hybrids lead to different relations between the X-ray-gamma-ray spectral index and the UV to X-ray-gamma-ray luminosity ratio. Such results have important implications for the analysis and modeling of individual AGN spectrum, which we will address in future papers. More importantly, we answer definitively the questions of the origin of the two-solution branches, whether there may be a third branch, and whether or not for some part of the parameter space the two branches will merge into a single, moderate optical depth solution. Such questions could not be addressed until now because the previous formulations

for the cooling flux equation apply only in the two opposite limits. The answer is simply that the bridging flux equation (16) indeed admits two and only two solutions for all relevant accretion parameters for β models. But for α models there may be zero, one, or two solutions depending on the values of L_* , α , and r . The significance and meaning of this finding is reported elsewhere. Which of the two solution branches does nature prefer? For the alpha models and for intermediate values of L_* , the answer seems to clear: the optically thick radiation pressure-dominated solution is secularly unstable whereas the other branch is stable. Hence we speculate that the optically thin hot solution would be preferred. But for β models and α models in the outer disk where the optically thick solution would be gas pressure-dominated, stability requirement does not discriminate between the two, so other factors may prevail. As it has been suggested before, the preconditioning of the accretion material may play a role (e.g., Ostriker et al. 1976). It seems that only truly time-dependent calculations with realistic boundary conditions at the outer disk boundary could settle such questions. Moreover, nature likely does not have a free choice between α or β model, either. Whether the azimuthal stress is more closely modeled by the gas pressure or total pressure may in fact depend on which branch the disk is in. But if the observed spectra are a true indicator of the disk structure, then both solutions might be relevant and coexist in space or time. The current approach will hopefully provide a new framework to test this hypothesis.

We are grateful to Chuck Dermer for his careful proofing of the manuscript and for helpful discussions. A. W. acknowledges useful discussions with Jim Pringle and Andrzej Zdziarski.

This work is performed under the auspices of the US DOE by the LLNL under contract number W-7405-ENG-48. A. W. is the incumbent of the Joseph and Ceilia Reskin Career Development Chair. A. W. is grateful for the hospitality of IGPP, LLNL and CSSA at Stanford University where part of this work was done. E. L. is partially supported by NASA NGR-05020-668 while visiting Stanford.

APPENDIX

In order to compare the new hot solutions with published cool solutions, we list here the analytic (or semianalytic) solutions for all quasi-thin accretion disk configurations discussed. These include the hot two-temperature and one-temperature α and β disks, cool α and β disks, and the outer blackbody solution (to which both cool solutions converge at low accretion rates or large enough radii) which is dominated by true absorption and gas pressure.

As in § 2, for the hot solutions we write the disk structure in terms of α ; for the β case one has to replace α by $(1 - P_*)\beta$.

1. HOT COMPTONIZED BREMSSTRAHLUNG SOLUTIONS

The hot two-temperature solution:

$$T_e = (5.8 \times 10^{10} \text{ K}) \alpha^{-4/9} L_*^{2/9} A^{-1/3} \Theta_*^{5/9} r^{-1/3}, \quad (\text{A1a})$$

$$\tau_{\text{es}} = 600 \alpha^{-1/9} L_*^{5/9} A^{-1/3} \Theta_*^{-1/9} r^{-5/6}, \quad (\text{A1b})$$

$$h/R = 0.17 \alpha^{-4/9} L_*^{2/9} A^{1/6} \Theta_*^{1/18} r^{1/6}, \quad (\text{A1c})$$

$$\rho = (5.8 \times 10^{-10} \text{ g cm}^{-3}) \alpha^{-1/3} L_*^{1/3} M_8^{-1} A^{1/2} \Theta_*^{-1/6} r^{-2}, \quad (\text{A1d})$$

$$T_i = (3.2 \times 10^{11} \text{ K}) \alpha^{-8/9} L_*^{4/9} A^{1/3} \Theta_*^{1/9} (1 - P_*) r^{-2/3}. \quad (\text{A1e})$$

The radiation-to-total pressure ratio P_* may be calculated from equation (14) while Θ_* is given by equations (11) and (31).

The hot one-temperature solution:

$$T_e = T_i = (4.9 \times 10^{11} \text{ K}) \alpha^{-1} L_*^{1/2} A^{1/2} (1 - P_*)^{5/4} r^{-3/4}, \quad (\text{A2a})$$

$$\tau_{\text{es}} = 390 L_*^{1/2} A^{-1/2} (1 - P_*)^{-1/4} r^{-3/4}, \quad (\text{A2b})$$

$$h/R = 0.19 \alpha^{-1/2} L_*^{1/4} A^{-1/4} (1 - P_*)^{-1/8}, \quad (\text{A2c})$$

$$\rho = (4.1 \times 10^{-10} \text{ g cm}^{-3}) \alpha^{1/2} L_*^{1/4} M_8^{-1} A^{-3/4} r^{-15/8}. \quad (\text{A2d})$$

2. COMPTONIZED SOFT PHOTONS SOLUTIONS

The hot two-temperature solution:

$$T_e = (3.8 \times 10^8 \text{ K}) \eta^{1/2} (1 + 4\Theta_e)^{-1/2} \Theta_*^{1/3} \alpha^{-1/6} L_*^{-1/6} r^{1/4}, \quad (\text{A3a})$$

$$\tau_{\text{es}} = 3.9 \eta^{1/2} (1 + 4\Theta_e)^{-1/2} \Theta_*^{-1/3} \alpha^{1/6} L_*^{1/6} r^{-1/4}, \quad (\text{A3b})$$

$$h/R = 0.24 \eta^{-1/4} \Theta_*^{1/6} \alpha^{-7/12} L_*^{5/12} (1 + 4\Theta_e)^{1/4} r^{-1/8}, \quad (\text{A3c})$$

$$\rho = 3.1 \times 10^{-13} \eta^{3/4} (1 + 4\Theta_e)^{-3/4} \Theta_*^{-1/2} \alpha^{3/4} M_8^{-1} L_*^{-1/4} r^{-9/8}, \quad (\text{A3d})$$

and

$$T_i = 4.1 \times 10^{13} \eta^{-1/2} \Theta_*^{1/3} (1 - P_*) \alpha^{3/2} L_*^{5/6} (1 + 4\Theta_e)^{1/2} r^{-5/4}, \quad (\text{A3e})$$

where η^{-1} is the ratio of the soft photon flux to the luminosity of the hot disk.

The hot one-temperature solution:

$$T = (2.5 \times 10^{19} \text{ K}) \eta^{-1} (1 + 4\Theta_e) \alpha^{-2} L_*^2 r^{-3}, \quad (\text{A4a})$$

$$\tau_{\text{es}} = 7.7 \times 10^{-6} \eta (1 + 4\Theta_e)^{-1} \alpha L_*^{-1} r^{3/2}, \quad (\text{A4b})$$

$$h/R = 40 \eta^{-1/2} \alpha^{-1} L_* r^{-1}, \quad (\text{A4c})$$

and

$$\rho = (8.5 \times 10^{-22} \text{ g cm}^{-3}) \eta^{3/2} (1 + 4\Theta_e)^{-3/2} \alpha^2 M_8^{-1} L_*^{-2} r^{3/2}. \quad (\text{A4d})$$

3. COOL SOLUTIONS

The cool radiation pressure-dominated α disk:

$$T = (4.5 \times 10^5 \text{ K}) \alpha^{-1/4} M_8^{-1/4} r^{-3/8}, \quad (\text{A5a})$$

$$\tau_{\text{es}} = 0.02 \alpha^{-1} L_*^{-1} r^{3/2}, \quad (\text{A5b})$$

$$h/R = 20 L_* r^{-1}, \quad (\text{A5c})$$

$$\rho = (1.7 \times 10^{-16} \text{ g cm}^{-3}) \alpha^{-1} L_*^{-2} M_8^{-1} r^{3/2}. \quad (\text{A5d})$$

The cool β disk:

$$T = (5.0 \times 10^7 \text{ K}) \beta^{-1/5} L_*^{2/5} M_8^{-1/5} r^{-9/10}, \quad (\text{A6a})$$

$$\tau_{\text{es}} = 3.9 \times 10^6 \beta^{-4/5} L_*^{3/5} M_8^{1/5} r^{-9/10}, \quad (\text{A6b})$$

$$h/R = 1.6 \times 10^{-5} L_* r^{-1}, \quad (\text{A6c})$$

$$\rho = (2.5 \times 10^{-8} \text{ g cm}^{-3}) \beta^{-4/5} L_*^{-2/5} M_8^{-4/5} r^{-3/5}. \quad (\text{A6d})$$

The cool blackbody gas pressure-dominated disk:

$$T = (8.3 \times 10^7 \text{ K}) \alpha^{-1/5} L_*^{3/10} M_8^{-1/5} r^{-3/4}, \quad (\text{A7a})$$

$$\tau_{\text{es}} = 1.9 \times 10^6 \alpha^{-4/5} L_*^{7/10} M_8^{1/5} r^{-3/4}, \quad (\text{A7b})$$

$$h/R = 3.0 \times 10^{-3} \alpha^{-1/10} L_*^{3/20} M_8^{-1/10} r^{1/8}, \quad (\text{A7c})$$

$$\rho = (1.2 \times 10^{-4} \text{ g cm}^{-3}) \alpha^{-7/10} L_*^{11/20} M_8^{-7/10} r^{-15/8}. \quad (\text{A7d})$$

REFERENCES

- Begelman, M., & Chiueh, T. 1988, ApJ, 332, 872
 Canfield, E., Howard, W. M., & Liang, E. P. 1987, ApJ, 323, 565
 Clarke, C. J. 1988, MNRAS, 235, 881
 Dermer, C. D., Liang, E. P., & Canfield, E. 1991, ApJ, 369, 410
 Eardley, D. M., & Lightman, A. P. 1975, ApJ, 200, 187
 Eardley, D. M., Lightman, A. P., Payne, D. G., & Shapiro, S. L. 1978, ApJ, 224, 53
 Guilbert, P. W., & Stepney, S. 1985, MNRAS, 212, 523
 Kusonose, M., & Takahara, F. 1989, PASJ, 41, 263
 Liang, E. P. 1991, ApJ, 367, 470

- Liang, E. P., & Dermer, C. D. 1988, ApJ, 325, L39
 Liang, E. P., & Price, R. H. 1977, ApJ, 218, 247
 Liang, E. P., & Thompson, K. A. 1979, MNRAS, 189, 421
 Liang, E. P., & Wandel, A. 1991, ApJ, 376, 746
 Lightman, A. P., & Eardley, D. M. 1974, ApJ, 187, L1
 Ling, J. C., Mahoney, W. A., Wheaton, W. A., & Jacobson, A. S. 1987, ApJ, 321, L117
 Novikov, I. D., & Thorne, K. S. 1973, in *Black Holes*, ed. B. & C. DeWitt (New York: Gordon & Breach), 343
 Ostriker, J. P., McCray, R., Weaver, R., & Yahil, A. 1976, ApJ, 208, L61
 Papaloizou, J. C. B., & Pringle, J. E. 1984, MNRAS, 208, 721
 Piran, T. 1978, ApJ, 221, 652
 Pozdnyakov, L. A., Sobol, I. M., & Sunyaev, R. A. 1976, *Soviet Astr.*, 54, 1246
 Pringle, J. E. 1976, MNRAS, 177, 65
 Pringle, J. E., & Rees, M. J. 1972, A&A, 21, 1
 Pringle, J. E., Rees, M. J., & Pacholczyk, A. 1973, A&A, 29, 179
 Rothschild, R. E., Mushotsky, R. F., Baity, W. A., Gruber, D. E., Matteson, J. L., & Peterson, L. E. 1983, ApJ, 269, 423
 Rybicki, G., & Lightman, A. P. 1979, *Radiative Processes in Astrophysics* (New York: John Wiley)
 Sakimoto, P. J., & Coroniti, F. V. 1981, ApJ, 247, 19
 Shakura, N. I., & Sunyaev, R. A. 1973, A&A, 24, 337
 ———. 1976, MNRAS, 175, 613
 Shapiro, S. L., Lightman, A. P., & Eardley, D. M. 1976, ApJ, 204, 187 (SLE)
 Spitzer, L., Jr., 1962, *Physics of Fully Ionized Gases* (New York: Wiley)
 Sun, W. H., & Malkan, M. A. 1986, in *New Insights in Astrophysics: Eight Years of Ultraviolet Astronomy with IUE*, ed. E. J. Rolfe (ESA SP-263) (Noordwijk: ESA), 641
 Svensson, R. 1984, MNRAS, 209, 175
 Thorne, K. S., & Price, R. H. 1975, ApJ, 195, L101
 Wandel, A., & Litwin, C. 1991, in preparation
 Wandel, A., & Petrosian, V. 1988, ApJ, 329, L11
 Wandel, A., & Urry, C. M. 1991, ApJ, 367, 78
 White, T. R., & Lightman, A. P. 1989, ApJ, 340, 1024
 Zdziarski, A. 1984, ApJ, 283, 842